An autonomous GNC strategy for asteroid impactor missions

Giovanni Purpura and Pierluigi Di Lizia

Abstract The Solar System features thousands of Near-Earth Asteroids that could be at collision risk with our planet in the future. Scientists are investigating the possibility of deflecting asteroids from their trajectory by means of a hyper-velocity impactor spacecraft. The aim of this research is to develop and simulate a GNC strategy to control the spacecraft towards the asteroid. The navigation is based on the use of a camera to estimate the relative position through image analysis and a filtering process. A zero-effort error strategy is adopted for the control. A simulator has been developed to render the simulated images online and test the GNC algorithms. The simulator is used to assess the performance of the strategy on different scenarios and perform a sensitivity analysis.

1 Introduction

The Solar System features thousands of Near-Earth Asteroids (NEA). Some of them could potentially have a collision with our planet in the future. The scientific community is currently investigating the possible actions to avert this event, which could lead to a catastrophic outcome. A possible strategy that is being considered is the deflection of the asteroid from its trajectory by impacting it with a spacecraft at very high velocity.

Several missions to asteroids or comets have already been realized or are under study by the major space agencies. In the followings, the missions that can be considered more relevant for this work are reported.

Giovanni Purpura
Politecnico di Milano, 20156 Milano, Italy, e-mail: giovanni.purpura@mail.polimi.it

Pierluigi Di Lizia
Politecnico di Milano, 20156 Milano, Italy, e-mail: pierluigi.dilizia@polimi.it

JAXA Hayabusa [11] was an exploration mission to asteroid 25143 Itokawa. It had autonomous optical navigation, using a target marker previously released on the asteroid. The camera image was processed using maximum correlation shifting and FFT. The control law allowed to approach from a prescribed direction.

NASA Deep Impact [10] was an Hypervelocity Asteroid Impact Vehicle to comet Tempel 1. For GNC it used AutoNav, a software developed for the previous mission Deep Space 1, which is able to perform image processing, orbit determination and maneuver computation. The image was processed by brightness centroiding, blobbing and scene analysis for site selection. It featured pulsed predictive control.

ESA Don Quijote [2] was a space probe concept to impact a NEA and determine the resulting momentum transfer. It was composed of an orbiter and an impactor. The orbiter could also perform surface analysis and mapping. It featured autonomous optical navigation for the impactor. This mission had been canceled in favor of AIDA.

ESA/NASA Asteroid Impact and Deflection mission (AIDA) [7] is a proposed pair of probes that would demonstrate an impact to change the motion of the binary NEA Didymos. NASA DART would impact the smallest body with the aid of a camera changing the speed by a fraction of 1 %. ESA Hera would arrive at Didymos in advance to study the asteroid and measure the effects of the impact.

The Space Mission Planning Advisory Group (SMPAG) [6] is a joint initiative established in 2013 between space agencies and other institutions, in order to prepare an international response to an asteroid impact threat. A preliminary work performed by the Italian Space Agency for SMPAG, which was aimed at defining and analyzing a test scenario for a deflection mission, was presented by Colombo et al. [3]. The chosen target for simulations is 2010 RF_{12}, a small NEA with significant probability of hitting the Earth. The work considered an asteroid in the orbit of 2010 RF_{12} with increased mass and diameter. The outcomes of the analysis was an optimal impact orbit and a preliminary list of components for the spacecraft.

Orbital insertion maneuvers are subjected to errors, therefore the spacecraft has to be controlled towards the target during the final phase of the mission. Since the camera can detect the asteroid only few hours before the impact, it is mandatory that Guidance, Navigation and Control (GNC) is performed autonomously. This paper aims at introducing a GNC strategy for the already defined scenario to 2010 RF_{12}.

The paper is organized as follows. The dynamics of the asteroid and the spacecraft are described in Sec. 2. Then, Sec. 3 presents the estimation process for the translational and rotational states by means of Kalman filters, focusing on the navigation camera and on the image analysis algorithm. The control strategy that allows the spacecraft to correct its course in order to impact the asteroid is defined in Sec. 4. Attitude control to keep the camera pointing towards the asteroid is introduced in Sec. 5. The defined equations and algorithms are used to develop a software simulator using MATLAB®, Simulink® and Blender®; the results of the simulations are reported in Sec. 6. In conclusion, the feasibility of the mission is discussed in Sec. 7, highlighting the reached goals and outlining the necessary future work.

2 Physical model

The dynamics of the asteroid and the spacecraft are modeled using classical rigid body dynamic equations, considering gravitational attraction from the Sun. The reduced timespan of the simulation allows to neglect the perturbation effect due to the mutual gravitational attraction.

2.1 Reference frames

Three reference frames will be used in order to describe the position and velocity of the asteroid and the spacecraft: the heliocentric ecliptic coordinate system, the Hill's frame and the spacecraft's body fixed frame.

2.1.1 Heliocentric ecliptic coordinate system

The heliocentric ecliptic coordinate system, denoted as E and with unit vectors $(\hat{\boldsymbol{\imath}}, \hat{\boldsymbol{\jmath}}, \hat{\boldsymbol{k}})$, has origin at the center of the Sun, its fundamental plane is the ecliptic plane and the $\hat{\boldsymbol{\imath}}$ axis points towards the vernal point. It is right handed and inertial.

2.1.2 Hill's rotating frame

Considering the position of the asteroid with respect to the Sun $\boldsymbol{r}_a$, its velocity $\dot{\boldsymbol{r}}_a$ and its specific angular momentum $\boldsymbol{h} = \boldsymbol{r}_a \times \dot{\boldsymbol{r}}_a$, the axes of the Hill's frame are:

$$\hat{\boldsymbol{r}} = \boldsymbol{r}_a / \|\boldsymbol{r}_a\|, \quad \hat{\boldsymbol{\theta}} = \hat{\boldsymbol{h}} \times \hat{\boldsymbol{r}}, \quad \hat{\boldsymbol{h}} = \boldsymbol{h} / \|\boldsymbol{h}\| \tag{1}$$

$\hat{\boldsymbol{r}}$ will always indicate the unit vector of $\boldsymbol{r}_a$, even if the subscript a is omitted. The Hill's frame will be centered in the asteroid's center of mass.

Since the asteroid is orbiting around the Sun with angular velocity $\boldsymbol{\omega}_a = \dot{\theta}\,\hat{\boldsymbol{h}}$, where θ is the true anomaly, the unit vectors $\hat{\boldsymbol{r}}$ and $\hat{\boldsymbol{\theta}}$ are time dependent; their time derivatives are:

$$\begin{cases} \dot{\hat{\boldsymbol{r}}} = \boldsymbol{\omega} \times \hat{\boldsymbol{r}} = \dot{\theta}\,\hat{\boldsymbol{\theta}} \\ \dot{\hat{\boldsymbol{\theta}}} = \boldsymbol{\omega} \times \hat{\boldsymbol{\theta}} = -\dot{\theta}\,\hat{\boldsymbol{r}} \end{cases} ; \quad \begin{cases} \ddot{\hat{\boldsymbol{r}}} = \ddot{\theta}\,\hat{\boldsymbol{\theta}} + \boldsymbol{\omega} \times (\dot{\theta}\,\hat{\boldsymbol{\theta}}) = \ddot{\theta}\,\hat{\boldsymbol{\theta}} - \dot{\theta}^2\,\hat{\boldsymbol{r}} \\ \ddot{\hat{\boldsymbol{\theta}}} = -\ddot{\theta}\,\hat{\boldsymbol{r}} + \boldsymbol{\omega} \times (-\dot{\theta}\,\hat{\boldsymbol{r}}) = -\ddot{\theta}\,\hat{\boldsymbol{r}} - \dot{\theta}^2\,\hat{\boldsymbol{\theta}} \end{cases} \tag{2}$$

2.1.3 Body fixed frame

This frame is fixed on the spacecraft, and is composed by its principal axes of inertia. Since the spacecraft attitude is not constant, this frame is non-inertial. This frame will be denoted using the letter B and the unit vectors $(\hat{\boldsymbol{x}}, \hat{\boldsymbol{y}}, \hat{\boldsymbol{z}})$.

The attitude of the spacecraft with respect to the ecliptic frame is represented using quaternions [4], implemented as column matrices:

$$\boldsymbol{q} = q_w + q_x\boldsymbol{i} + q_y\boldsymbol{j} + q_z\boldsymbol{k}, \qquad \boldsymbol{q} = \begin{bmatrix} q_w & q_x & q_y & q_z \end{bmatrix}^T \tag{3}$$

For a rotation θ around an unit vector (u_x, u_y, u_z) the quaternion will be:

$$\boldsymbol{q} = \cos(\theta/2) + (u_x\boldsymbol{i} + u_y\boldsymbol{j} + u_z\boldsymbol{k})\sin(\theta/2) \tag{4}$$

A vector $\boldsymbol{v}$ can be rotated using the Hamilton product $\times$:

$$\begin{bmatrix} 0 \\ \boldsymbol{v}^B \end{bmatrix} = \boldsymbol{q}^* \times \begin{bmatrix} 0 \\ \boldsymbol{v}^E \end{bmatrix} \times \boldsymbol{q} \tag{5}$$

The rotation matrix that allows to convert a vector from the ecliptic frame to the body fixed frame can be obtained from the rotation quaternion as:

$$\mathbf{A}_{B/E} = \begin{bmatrix} q_{\mathrm{w}}^2 + q_{\mathrm{x}}^2 - q_{\mathrm{y}}^2 - q_{\mathrm{z}}^2 & 2(q_{\mathrm{x}}\,q_{\mathrm{y}} + q_{\mathrm{w}}\,q_{\mathrm{z}}) & 2(q_{\mathrm{x}}\,q_{\mathrm{z}} - q_{\mathrm{w}}\,q_{\mathrm{y}}) \\ 2(q_{\mathrm{x}}\,q_{\mathrm{y}} - q_{\mathrm{w}}\,q_{\mathrm{z}}) & q_{\mathrm{w}}^2 - q_{\mathrm{x}}^2 + q_{\mathrm{y}}^2 - q_{\mathrm{z}}^2 & 2(q_{\mathrm{y}}\,q_{\mathrm{z}} + q_{\mathrm{w}}\,q_{\mathrm{x}}) \\ 2(q_{\mathrm{x}}\,q_{\mathrm{z}} + q_{\mathrm{w}}\,q_{\mathrm{y}}) & 2(q_{\mathrm{y}}\,q_{\mathrm{z}} - q_{\mathrm{w}}\,q_{\mathrm{x}}) & q_{\mathrm{w}}^2 - q_{\mathrm{x}}^2 - q_{\mathrm{y}}^2 + q_{\mathrm{z}}^2 \end{bmatrix} \tag{6}$$

2.2 Asteroid translational dynamics

The asteroid is assumed to be subjected only to Sun's gravity: the other perturbing forces are assumed to have negligible effects in the short timespan of the simulation. Consequently, the asteroid is on a Keplerian orbit and its motion can be described using its true anomaly θ. The dynamical equations can be derived from Newton's gravitation law:

$$\ddot{\boldsymbol{r}}_{\boldsymbol{a}} = -\frac{\mu}{r_a^3}\boldsymbol{r}_a = -\frac{\mu}{r_a^2}\hat{\boldsymbol{r}} \tag{7}$$

where μ is the standard gravitational parameter of the Sun and $\hat{\boldsymbol{r}} = \boldsymbol{r}_a/r_a$ as previously defined. The acceleration can be obtained by differentiating twice the position $\boldsymbol{r}_a$:

$$\ddot{\boldsymbol{r}}_a = \left(\ddot{r}_a - r_a\dot{\theta}^2\right)\hat{\boldsymbol{r}} + \left(r_a\ddot{\theta} + 2\dot{r}_a\dot{\theta}\right)\hat{\boldsymbol{\theta}} \tag{8}$$

Substituting (8) into (7), and considering that $\hat{\boldsymbol{r}}$ and $\hat{\boldsymbol{\theta}}$ are orthogonal, the system of coupled nonlinear ordinary differential equations that describe the orbit of the asteroid around the Sun is obtained:

$$\ddot{r}_a = r_a\,\dot{\theta}^2 - \frac{\mu}{r_a^2}; \qquad \ddot{\theta} = -2\frac{\dot{r}_a}{r_a}\dot{\theta} \tag{9}$$

2.3 Spacecraft dynamics

The motion of the spacecraft is assumed to be governed by the Sun's gravitational force and the control force:

$$\ddot{\boldsymbol{r}}_s = -\frac{\mu}{r_s^3}\boldsymbol{r}_s + \frac{\boldsymbol{f}}{m_s} \tag{10}$$

where $\boldsymbol{r}_s$ is position vector of the spacecraft with respect to the Sun, $\boldsymbol{f}$ is the control force and m_s is the mass of the spacecraft. The control force will be computed in the body frame, while the dynamic equations of the spacecraft will be written in the Hill's frame. The conversion from one frame to the other is achieved using the rotation matrix $\mathbf{A}_{H/B}$, that can be obtained from the matrices that relate the Hill's and the body frames to the ecliptic frame ($\mathbf{A}_{H/E}$ and $\mathbf{A}_{B/E}$ respectively):

$$\boldsymbol{f}^H = \begin{bmatrix} f_x & f_y & f_z \end{bmatrix}_H^T = \mathbf{A}_{H/B}\,\boldsymbol{f}^B, \quad \mathbf{A}_{H/B} = \mathbf{A}_{H/E}\,\mathbf{A}_{B/E}^T \tag{11}$$

It is convenient to use the relative position vector between spacecraft and asteroid:

$$\boldsymbol{\rho} = \boldsymbol{r}_s - \boldsymbol{r}_a = x\hat{\boldsymbol{r}} + y\hat{\boldsymbol{\theta}} + z\hat{\boldsymbol{h}} \tag{12}$$

Considering that the second derivative of $\boldsymbol{r}_s$ is $\ddot{\boldsymbol{r}}_s = \ddot{\boldsymbol{r}}_a + \ddot{\boldsymbol{\rho}}$ and using equations Eq. 7 and 10, the relative translational dynamics can be obtained [12, 5]:

$$\begin{cases} \ddot{x} - 2\dot{\theta}\dot{y} - \ddot{\theta}y - \dot{\theta}^2 x = -\mu\,(r + x)/r_s^3 + f_x/m_s + \mu/r_a^2 \\ \ddot{y} + 2\dot{\theta}\dot{x} + \ddot{\theta}x - \dot{\theta}^2 y = -\mu\,(\quad y \quad)/r_s^3 + f_y/m_s \\ \ddot{z} \qquad\qquad\qquad\quad = -\mu\,(\quad z \quad)/r_s^3 + f_z/m_s \end{cases} \tag{13}$$

The attitude is governed by Euler's rotation equation and by quaternion kinematics ([4]), with $\boldsymbol{\omega}^B$ angular velocity, $\mathbf{I}^B$ inertia matrix and $\boldsymbol{m}^B$ applied torque:

$$\mathbf{I}^B\dot{\boldsymbol{\omega}}^B + \boldsymbol{\omega}^B \times \left(\mathbf{I}^B\boldsymbol{\omega}^B\right) = \boldsymbol{m}^B; \quad \dot{\boldsymbol{q}} = \frac{1}{2}\begin{bmatrix} 0 \\ \boldsymbol{\omega}^B \end{bmatrix} \times \boldsymbol{q} \tag{14}$$

3 Navigation

The relative attitude and position of the spacecraft with respect to the asteroid must be estimated to control the trajectory until impact. A star tracker, a gyroscope and a navigation camera allow to reconstruct the state of the system using Kalman filters.

3.1 Navigation camera

The image acquired by the navigation camera is simulated using the Blender® software, considering the relative position of the spacecraft with respect to the asteroid and the camera's optical properties. The image is then interpreted by a processing algorithm that returns the angular position of the asteroid in the FOV. These angles are then used by the Kalman filter to estimate the translational state.

As reported in Fig. 1, the image is read into a matrix of 8-bit values (from 0 for black to 255 for white). A threshold filter is applied and a circle is fitted on the illuminated border of the asteroid. This gives an estimation of the center of the asteroid in the FOV. A more detailed description of these operations follows.

Fig. 1 Image analysis algorithm

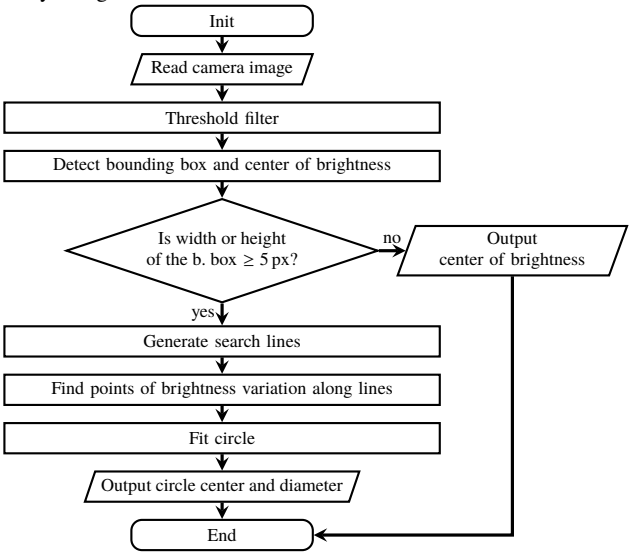

Brightness threshold The pixels beyond a given brightness threshold are determined. This returns a boolean matrix, where the asteroid's image is formed by ones and the background is translated into zeros.

Bounding box and brightness centroiding The matrix is scanned to find the smallest box that contains all the illuminated pixels to locate the asteroid in the image. A weighted mean of the position of the illuminated pixels gives the center of brightness (COB), that serves as a preliminary estimation of the asteroid center. With **B** as the boolean matrix (true and false are 1 and 0), the COB can be computed:

$$\boldsymbol{CoB} = \left(\frac{\sum_{i,j} i\, \mathbf{B}(i,j)}{\sum_{i,j} \mathbf{B}(i,j)}, \frac{\sum_{i,j} j\, \mathbf{B}(i,j)}{\sum_{i,j} \mathbf{B}(i,j)} \right) \tag{15}$$

Circular fitting A possible way to mitigate the error between the center of brightness and center of mass is to guess the shape of the asteroid. When its image is large enough, it is possible to fit a circular shape using the illuminated points; then, the center of the circle is used instead of the COB. The determination of the points on the border is based on search lines parallel to the direction of the Sun rays, in order to use only the illuminated edge of the asteroid.

The equation of a circle with radius r centered in (c_x, c_y) is:

$$x^2 + y^2 = 2\,c_x\,x + 2\,c_y\,y + r^2 - (c_x^2 + c_y^2) \tag{16}$$

This equation, applied to each fitting point (x_i, y_i), leads to the linear system:

$$\begin{bmatrix} x_1 & y_1 & 1 \\ \vdots & \vdots & \vdots \\ x_N & y_N & 1 \end{bmatrix} \mathbf{a} = \begin{bmatrix} x_1^2 + y_1^2 \\ \vdots \\ x_N^2 + y_N^2 \end{bmatrix}; \quad \text{with solution:} \quad \boldsymbol{a} = \begin{bmatrix} 2\,c_x \\ 2\,c_y \\ r^2 - (c_x^2 + c_y^2) \end{bmatrix} \tag{17}$$

With least-squares approximation it is possible to obtain $\boldsymbol{a}$, i.e. the parameters in Eq. 16. The resulting center and diameter are used to determine the position and the size of the asteroid, using optical relations that will be introduced afterwards.

Other shapes could be used, for instance elliptical fitting could be ideally more suitable for asteroids with elongated shape. In this case, the fitting parameters are the position of the center, the length of the axes and an orientation angle. However, in the frame of preliminary tests, elliptical fitting turned out to provide worse performances due to the concentration of all the fitting points in the illuminated side of the asteroid. This is evident in Fig. 2 (left), where the obtained circle and ellipse are overlaid. The circle fits well the shape of the asteroid, while the resulting ellipse is twice the correct size, with a center almost outside of the asteroid. The adoption of elliptical shapes in the fitting process will be investigated further in future studies.

The algorithms have also been tested on asteroid Itokawa (Fig. 2, right): both the circular and the elliptical fits give a smaller estimation of the size of the asteroid, leading to an estimation of the center that shifts towards the illuminated border.

Fig. 2 Different fitting methods applied to Bennu and Itokawa (straight lines = scan lines, yellow circles = detected fitting points, green dashed line = reference circle with 550 m diameter, red line = fitted circle, light blue line = fitted ellipse, black $*$ = center of brightness (COB))

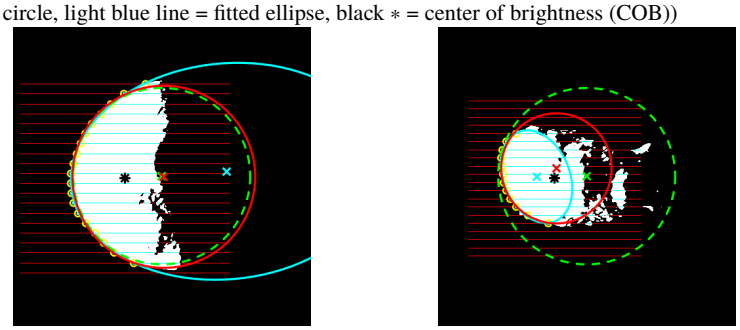

3.1.1 Optical properties and relations

The mathematical relations that allow to convert the position of the asteroid in the image to a measurement that can be used by the Kalman filter are reported below.

Focal Length Assuming that the asteroid distance is much longer than the size of the camera, the Focal Length (FL) is the distance between the sensor and the lens.

Field Of View The Field Of View (FOV) is the solid angle detected by the camera.

Resolution The resolution (Res) is the number of pixels on the sensor of the camera, that will be supposed square (in size and resolution).

Size of the sensor The length of its sides can be obtained from the relation:

$$\text{SensorSideLength} = 2 \times \text{FL} \times \tan\left(\text{FOV}/2\right) \tag{18}$$

The meaning of this equation is that to have a longer FL, while keeping the same FOV, the sensor must be enlarged proportionally; otherwise, the FOV is reduced.

Size of a pixel Since the sensor is a uniform grid composed by Res-by-Res pixels, each of them is a square with sides of length:

$$\text{PixelSideLength} = \text{SensorSideLength}/\text{Res} \tag{19}$$

Angular measurements The image is stored in terms of a square matrix of size Res-by-Res. The following procedure is adopted to retrieve the physical position of a pixel, in terms of the azimuth and elevation angles. First, the index range is centered:

$$[1; \text{Res}] \rightarrow [-(\text{Res} - 1)/2; +(\text{Res} - 1)/2] \tag{20}$$

Then, a Cartesian coordinate centered on the sensor can be obtained by multiplying the range in Eq. 20 by the size of a pixel. The ratio of the position on the sensor with respect to the focal length represents the tangent of the angle in the camera FOV, that will be considered equal to the angle itself. The overall formula that allows to convert the position of a pixel (PixelPos) in the range $[1; \text{Res}]$ to a camera angle is:

$$\text{CameraAngles} = (\text{PixelPos} - 0.5\,\text{px} - \text{Res}/2) \times \text{PixelSideLength}/\text{FL} \tag{21}$$

Image size Since the diameter of the asteroid and its projection on the sensor form, with the lens, two triangles in similarity relationship, it is possible to convert the physical size (AstDiameter) to the projected size on the sensor (AstImgDiameter):

$$\text{AstImgDiameter} = \text{AstDiameter} \times \text{FL}/\text{Distance} \tag{22}$$

The size in pixels ($\text{AstImgDiameter}_{\text{Px}}$) can be computed by dividing the physical size of the image on the sensor by the size of a pixel:

$$\text{AstImgDiameter}_{\text{Px}} = \frac{\text{AstImgDiameter}}{\text{PixelSideLength}} = \frac{\text{AstImgDiameter} \times \text{Res}}{\text{SensorSideLength}} \tag{23}$$

3.2 Filtering

The implemented feedback control depends on the state of the system, yet the spacecraft does not have direct measurements of it. In order to obtain sufficiently accurate estimates of the spacecraft state it is necessary to use the measurements given by the sensors, which are processed by a Kalman filter. Kalman filters need the state space equations and the measurements of the system:

$$\dot{\boldsymbol{x}}(t) = \boldsymbol{f}\left(\boldsymbol{x}(t)\right) + \boldsymbol{u}(t); \quad \tilde{\boldsymbol{y}}(t) = \boldsymbol{h}\left(\boldsymbol{x}(t), t\right) + \boldsymbol{v}(t) \quad \boldsymbol{v}(t) \sim \mathcal{N}\left(\mathbf{0}, \mathbf{R}(t)\right) \tag{24}$$

where $\boldsymbol{x}$ is the state vector, $\boldsymbol{u}$ is the input (the control action) and $\tilde{\boldsymbol{y}}$ is the measurement from the sensor with additive noise $\boldsymbol{v}$. The dynamics of the system have been assumed to be affine in the control action.

Extended Kalman filters need also a linearized version of the equations:

$$\dot{\boldsymbol{x}}(t) = \mathbf{F}(t)\boldsymbol{x}(t) + \boldsymbol{u}(t); \quad \tilde{\boldsymbol{y}}(t) = \mathbf{H}(t)\boldsymbol{x}(t) + \boldsymbol{v}(t) \quad \boldsymbol{v}(t) \sim \mathcal{N}\left(\mathbf{0}, \mathbf{R}(t)\right) \tag{25}$$

where $\mathbf{F}$ and $\mathbf{H}$ are the Jacobian matrices of $\boldsymbol{f}$ and $\boldsymbol{h}$ with respect to the state.

3.2.1 Translation state equations

The translational state of the system is the position of the spacecraft with respect to the asteroid written in the Hill's reference frame $\boldsymbol{\rho}$:

$$\boldsymbol{x} = \begin{bmatrix} \boldsymbol{\rho} \\ \dot{\boldsymbol{\rho}} \end{bmatrix}, \quad \dot{\boldsymbol{x}} = \begin{bmatrix} \dot{\boldsymbol{\rho}} \\ \ddot{\boldsymbol{\rho}} \end{bmatrix}; \quad \mathbf{F} = \frac{\partial \dot{\boldsymbol{x}}}{\partial \boldsymbol{x}} = \begin{bmatrix} \frac{\partial \dot{\boldsymbol{\rho}}}{\partial \boldsymbol{\rho}} & \frac{\partial \dot{\boldsymbol{\rho}}}{\partial \dot{\boldsymbol{\rho}}} \\ \frac{\partial \ddot{\boldsymbol{\rho}}}{\partial \boldsymbol{\rho}} & \frac{\partial \ddot{\boldsymbol{\rho}}}{\partial \dot{\boldsymbol{\rho}}} \end{bmatrix} \tag{26}$$

Considering that the state affects also $\boldsymbol{r}_s$ since $\boldsymbol{r}_s = \boldsymbol{r}_a + \boldsymbol{\rho}$, the Jacobian is:

$$\frac{\partial \dot{\boldsymbol{\rho}}}{\partial \boldsymbol{\rho}} = \mathbf{0}_3, \; \frac{\partial \dot{\boldsymbol{\rho}}}{\partial \dot{\boldsymbol{\rho}}} = \mathbf{I}_3, \; \frac{\partial \ddot{\boldsymbol{\rho}}}{\partial \boldsymbol{\rho}} = \begin{bmatrix} \dot{\theta}^2 & \ddot{\theta} & 0 \\ -\ddot{\theta} & \dot{\theta}^2 & 0 \\ 0 & 0 & 0 \end{bmatrix} - \frac{\mu}{r_s^3}\mathbf{I}_3 + 3\frac{\mu}{r_s^5}\left[\boldsymbol{r_s}\boldsymbol{r_s}^T\right], \; \frac{\partial \ddot{\boldsymbol{\rho}}}{\partial \dot{\boldsymbol{\rho}}} = \begin{bmatrix} 0 & 2\dot{\theta} & 0 \\ -2\dot{\theta} & 0 & 0 \\ 0 & 0 & 0 \end{bmatrix} \tag{27}$$

The measurements for the camera are the azimuth and elevation of the asteroid in the FOV; using the previously presented optical relations, they can be computed as:

$$\boldsymbol{h} = \begin{bmatrix} \gamma & \alpha \end{bmatrix}^T = \begin{bmatrix} -a/c & +b/c \end{bmatrix}^T \tag{28}$$

where (a, b, c) is Line Of Sight (LOS) unit vector in the body frame:

$$\hat{\boldsymbol{\rho}}^B = \begin{bmatrix} a & b & c \end{bmatrix}_B^T = \boldsymbol{\rho}^B/\rho = \mathbf{A}_{B/H}\boldsymbol{\rho}^H/\rho = \mathbf{A}_{B/H}\hat{\boldsymbol{\rho}}^H \tag{29}$$

The measurement equation can be now expressed as:

$$\boldsymbol{h} = \boldsymbol{h}(\hat{\boldsymbol{\rho}}^B) = \boldsymbol{h}(\mathbf{A}_{B/H}(\boldsymbol{q})\boldsymbol{\rho}^H/\rho) \tag{30}$$

It is now necessary to compute the Jacobian matrix of the measurement function with respect to the state of the system:

$$\mathbf{H} = \frac{\partial \boldsymbol{h}}{\partial \boldsymbol{\rho}^H} = \frac{\partial \boldsymbol{h}}{\partial \hat{\boldsymbol{\rho}}^B} \frac{\partial \hat{\boldsymbol{\rho}}^B}{\partial \hat{\boldsymbol{\rho}}^H} \frac{\partial \hat{\boldsymbol{\rho}}^H}{\partial \boldsymbol{\rho}^H} \tag{31}$$

$$\frac{\partial \boldsymbol{h}}{\partial \hat{\boldsymbol{\rho}}^B} = \begin{bmatrix} -1/c & 0 & a/c^2 \\ 0 & 1/c & -b/c^2 \end{bmatrix}, \quad \frac{\partial \hat{\boldsymbol{\rho}}^B}{\partial \hat{\boldsymbol{\rho}}^H} = \mathbf{A}_{B/H} \tag{32}$$

$$\frac{\partial \hat{\boldsymbol{\rho}}}{\partial \boldsymbol{\rho}} = \frac{\partial \left(\boldsymbol{\rho} / \sqrt{\boldsymbol{\rho}^T \boldsymbol{\rho}} \right)}{\partial \boldsymbol{\rho}} = \frac{\mathbf{I}_3 \sqrt{\boldsymbol{\rho}^T \boldsymbol{\rho}} - \boldsymbol{\rho} \boldsymbol{\rho}^T / \sqrt{\boldsymbol{\rho}^T \boldsymbol{\rho}}}{\boldsymbol{\rho}^T \boldsymbol{\rho}} = \frac{\rho^2 \mathbf{I}_3 - \boldsymbol{\rho} \boldsymbol{\rho}^T}{\rho^3} \tag{33}$$

The derivatives of the measurement with respect to the rotation quaternion are:

$$\frac{\partial \boldsymbol{h}}{\partial \boldsymbol{q}} = \frac{\partial \boldsymbol{h}}{\partial \hat{\boldsymbol{\rho}}^B} \left[\frac{\partial \mathbf{A}_{B/H}}{\partial q_{\mathrm{w}}} \hat{\boldsymbol{\rho}}^H \ \frac{\partial \mathbf{A}_{B/H}}{\partial q_{\mathrm{x}}} \hat{\boldsymbol{\rho}}^H \ \frac{\partial \mathbf{A}_{B/H}}{\partial q_{\mathrm{y}}} \hat{\boldsymbol{\rho}}^H \ \frac{\partial \mathbf{A}_{B/H}}{\partial q_{\mathrm{z}}} \hat{\boldsymbol{\rho}}^H \right] \tag{34}$$

The derivatives of $\mathbf{A}_{B/H}$ can be derived considering Eq. 6.

Since the estimated state is expressed with respect to the inertial frame by $\boldsymbol{q}_{B/E}$, while the quaternion needed for the previous equation is between body frame and Hill's frame ($\boldsymbol{q}_{B/H}$), it is necessary to convert the rotation and its covariance Σ:

$$\boldsymbol{q}_{B/E} = \boldsymbol{q}_{B/H} \times \boldsymbol{q}_{H/E} \quad \Longrightarrow \quad \boldsymbol{q}_{B/E} = \boldsymbol{q}_{B/E} \times \boldsymbol{q}^*_{H/E} \tag{35}$$

$$\Sigma_{\boldsymbol{q}_{B/H}} = \mathbf{J}_{\boldsymbol{q}} \, \Sigma_{\boldsymbol{q}_{B/H}} \, \mathbf{J}_{\boldsymbol{q}}^T; \quad \mathbf{J}_q = \frac{\partial \left(\boldsymbol{q}_{B/E} \times \boldsymbol{q}^*_{H/E} \right)}{\partial \boldsymbol{q}_{H/E}} = \begin{bmatrix} +q_{\mathrm{w}} & +q_{\mathrm{x}} & +q_{\mathrm{y}} & +q_{\mathrm{z}} \\ -q_{\mathrm{x}} & +q_{\mathrm{w}} & -q_{\mathrm{z}} & +q_{\mathrm{y}} \\ -q_{\mathrm{y}} & +q_{\mathrm{z}} & +q_{\mathrm{w}} & -q_{\mathrm{x}} \\ -q_{\mathrm{z}} & -q_{\mathrm{y}} & +q_{\mathrm{x}} & +q_{\mathrm{w}} \end{bmatrix} \tag{36}$$

3.2.2 Rotation state equations

The state of the system for the rotational dynamics is composed of its angular velocity $\boldsymbol{\omega}^B$ and its attitude quaternion $\boldsymbol{q}_{B/E}$ (with respect to the inertial reference frame):

$$\boldsymbol{x} = \begin{bmatrix} \boldsymbol{\omega} \\ \boldsymbol{q} \end{bmatrix}, \quad \dot{\boldsymbol{x}} = \begin{bmatrix} \dot{\boldsymbol{\omega}} \\ \dot{\boldsymbol{q}} \end{bmatrix}; \quad \mathbf{F} = \frac{\partial \dot{\boldsymbol{x}}}{\partial \boldsymbol{x}} = \begin{bmatrix} \frac{\partial \dot{\boldsymbol{\omega}}}{\partial \boldsymbol{\omega}} & \frac{\partial \dot{\boldsymbol{\omega}}}{\partial \boldsymbol{q}} \\ \frac{\partial \dot{\boldsymbol{q}}}{\partial \boldsymbol{\omega}} & \frac{\partial \dot{\boldsymbol{q}}}{\partial \boldsymbol{q}} \end{bmatrix} \tag{37}$$

The superscript ^{B} and the subscript $_{B/E}$ are omitted to simplify the notation. The Jacobian can be obtained from the rotational equations (14).

Measurement: star tracker Star trackers acquire images of deep space in order to reconstruct the attitude of the spacecraft using the position of the stars in their FOV. Within this work, the star tracker provides directly angular measurements of the spacecraft attitude. Choosing for example Tait-Bryan angles, that describe the

rotations as $\mathbf{R}_z(\psi)\mathbf{R}_y(\theta)\mathbf{R}_x(\phi)$ ([1, p. 39]), the measurements are:

$$\boldsymbol{h} = \begin{bmatrix}\phi\\ \theta\\ \psi\end{bmatrix} = \begin{bmatrix}\text{atan2}\,(a_1, a_2)\\ \text{asin}\,(a_3)\\ \text{atan2}\,(a_4, a_5)\end{bmatrix} \quad \text{with}: \quad \begin{cases} a_1 = q_\text{w}\, q_\text{x} + q_\text{y}\, q_\text{z} \\ a_2 = 1/2 - (q_\text{x}^2 + q_\text{y}^2) \\ a_3 = 2\,(q_\text{w}\, q_\text{y} - q_\text{z}\, q_\text{x}) \\ a_4 = q_\text{w}\, q_\text{z} + q_\text{x}\, q_\text{y} \\ a_5 = 1/2 - (q_\text{y}^2 + q_\text{z}^2) \end{cases} \tag{38}$$
$$\mathbf{H} = \frac{\partial \boldsymbol{h}}{\partial \boldsymbol{x}} = \begin{bmatrix}\mathbf{0}_3 & \dfrac{\partial \boldsymbol{h}}{\partial \boldsymbol{q}}\end{bmatrix}$$

Measurement: gyroscope The gyroscope measurement function and Jacobian are:

$$\boldsymbol{h} = \boldsymbol{\omega}^B; \quad \mathbf{H} = \frac{\partial \boldsymbol{h}}{\partial \boldsymbol{x}} = \begin{bmatrix}\mathbf{I}_3 & \mathbf{0}_{3,4}\end{bmatrix} \tag{39}$$

3.2.3 Consider Extended Kalman filter equations

The reconstruction of the state is performed using a continuous-discrete Consider Extended Kalman Filter (CEKF) [13]. The CEKF is an extension of the EKF that allows to account for the effect of a bias in the estimation directly in the propagated covariance matrix. In this way, it is possible to take into consideration that the center of mass of the asteroid may not coincide with the center identified in the image. This can be modeled as a displacement $\bar{\boldsymbol{\rho}}$ added to the estimated position $\tilde{\boldsymbol{\rho}}$:

$$\boldsymbol{\rho}(t) = \tilde{\boldsymbol{\rho}}(t) + \bar{\boldsymbol{\rho}}, \quad \boldsymbol{\rho}^H = \begin{bmatrix}x & y & z\end{bmatrix}^T, \quad \tilde{\boldsymbol{\rho}}^H = \begin{bmatrix}\tilde{x} & \tilde{y} & \tilde{z}\end{bmatrix}^T, \quad \bar{\boldsymbol{\rho}}^H = \begin{bmatrix}\bar{x} & \bar{y} & \bar{z}\end{bmatrix}^T \tag{40}$$

The term $\bar{\boldsymbol{\rho}}$ is modeled as a Gaussian zero-mean random error. Considering Eq. 40 the previously derived system Eq. 13 becomes:

$$\begin{cases} \ddot{x} - 2\dot{\theta}\dot{y} - \ddot{\theta}(\tilde{y} + \bar{y}) - \dot{\theta}^2(\tilde{x} + \bar{x}) = -\mu\,(r + \tilde{x} + \bar{x})/r_s^3 + f_x/m_{SC} + \mu/r_c^2 \\ \ddot{y} + 2\dot{\theta}\dot{x} + \ddot{\theta}(\tilde{x} + \bar{x}) - \dot{\theta}^2(\tilde{y} + \bar{y}) = -\mu\,(\quad \tilde{y} + \bar{y} \quad)/r_s^3 + f_y/m_{SC} \\ \ddot{z} \qquad\qquad\qquad\qquad\qquad\qquad\quad = -\mu\,(\quad \tilde{z} + \bar{z} \quad)/r_s^3 + f_z/m_{SC} \end{cases} \tag{41}$$
$$\text{with: } r_s = [(r_a + \tilde{x} + \bar{x})^2 + (\tilde{y} + \bar{y})^2 + (\tilde{z} + \bar{z})^2]^{1/2}$$

The state that is reconstructed is therefore:

$$\boldsymbol{x} = \begin{bmatrix}\tilde{\boldsymbol{\rho}} & \dot{\tilde{\boldsymbol{\rho}}}\end{bmatrix}^T, \quad \dot{\boldsymbol{x}} = \begin{bmatrix}\dot{\tilde{\boldsymbol{\rho}}} & \ddot{\tilde{\boldsymbol{\rho}}}\end{bmatrix}^T; \quad \dot{\boldsymbol{x}}(t) = \boldsymbol{f}\,(\boldsymbol{x}(t), \bar{\boldsymbol{\rho}}, t) + \boldsymbol{u}(t) \tag{42}$$

State propagation is not affected by the introduction of $\bar{\boldsymbol{\rho}}$, since its estimate is zero. The Jacobian $\mathbf{F}$ remains as previously derived and the Jacobian with respect to the displacement $\bar{\boldsymbol{\rho}}$, $\mathbf{B}_{\bar{\boldsymbol{\rho}}}$, is the left half of $\mathbf{F}$ from Eq. 26, thanks to the fact that partial derivatives of a function of $\boldsymbol{\rho}$ with respect to $\boldsymbol{\rho}$, $\tilde{\boldsymbol{\rho}}$ or $\bar{\boldsymbol{\rho}}$, are identical:

$$\frac{\partial f(\boldsymbol{\rho})}{\partial \tilde{\boldsymbol{\rho}}} = \frac{\partial f(\boldsymbol{\rho})}{\partial \boldsymbol{\rho}}\frac{\partial \boldsymbol{\rho}}{\partial \tilde{\boldsymbol{\rho}}} = \frac{\partial f(\boldsymbol{\rho})}{\partial \boldsymbol{\rho}}, \quad \frac{\partial f(\boldsymbol{\rho})}{\partial \bar{\boldsymbol{\rho}}} = \frac{\partial f(\boldsymbol{\rho})}{\partial \boldsymbol{\rho}}\frac{\partial \boldsymbol{\rho}}{\partial \bar{\boldsymbol{\rho}}} = \frac{\partial f(\boldsymbol{\rho})}{\partial \boldsymbol{\rho}} \tag{43}$$

Table 1 Consider Extended Kalman Filter equations

Model	$\dot{\boldsymbol{x}}(t) = \boldsymbol{f}\left(\boldsymbol{x}(t), \bar{\boldsymbol{\rho}}, t\right) + \boldsymbol{u}(t); \quad \tilde{\boldsymbol{y}}(t) = \boldsymbol{h}(\boldsymbol{x}(t), \bar{\boldsymbol{\rho}}, t) + \boldsymbol{v}(t); \quad \boldsymbol{v}(t) \sim \mathcal{N}(\mathbf{0}, \mathbf{R}(t))$
Gain	$\mathbf{K} = \left(\mathbf{P}^-_{\boldsymbol{xx}}\mathbf{H}^T_{\boldsymbol{x}} + \mathbf{P}^-_{\boldsymbol{x}\bar{\boldsymbol{\rho}}}\mathbf{H}^T_{\bar{\boldsymbol{\rho}}}\right)\left(\mathbf{H}_{\boldsymbol{x}}\mathbf{P}^-_{\boldsymbol{xx}}\mathbf{H}^T_{\boldsymbol{x}} + \mathbf{H}_{\boldsymbol{x}}\mathbf{P}^-_{\boldsymbol{x}\bar{\boldsymbol{\rho}}}\mathbf{H}^T_{\bar{\boldsymbol{\rho}}} + \mathbf{H}_{\bar{\boldsymbol{\rho}}}\mathbf{P}^-_{\bar{\boldsymbol{\rho}}\boldsymbol{x}}\mathbf{H}^T_{\boldsymbol{x}} + \mathbf{H}_{\bar{\boldsymbol{\rho}}}\mathbf{P}^-_{\bar{\boldsymbol{\rho}}\bar{\boldsymbol{\rho}}}\mathbf{H}^T_{\bar{\boldsymbol{\rho}}} + \mathbf{R}\right)^{-1}$
Update	$\hat{\boldsymbol{x}}^+ = \hat{\boldsymbol{x}}^- + \mathbf{K}\left(\tilde{\boldsymbol{y}} - \mathbf{H}_{\boldsymbol{x}}\hat{\boldsymbol{x}}^- - \mathbf{H}_{\bar{\boldsymbol{\rho}}}\hat{\bar{\boldsymbol{\rho}}}\right)$ $\mathbf{P}^+_{\boldsymbol{xx}} = (\mathbf{I} - \mathbf{K}\mathbf{H}_{\boldsymbol{x}})\mathbf{P}^-_{\boldsymbol{xx}} - \mathbf{K}\mathbf{H}_{\bar{\boldsymbol{\rho}}}\mathbf{P}^-_{\bar{\boldsymbol{\rho}}\boldsymbol{x}}; \quad \mathbf{P}^+_{\boldsymbol{x}\bar{\boldsymbol{\rho}}} = (\mathbf{I} - \mathbf{K}\mathbf{H}_{\boldsymbol{x}})\mathbf{P}^-_{\boldsymbol{x}\bar{\boldsymbol{\rho}}} - \mathbf{K}\mathbf{H}_{\bar{\boldsymbol{\rho}}}\mathbf{P}_{\bar{\boldsymbol{\rho}}\bar{\boldsymbol{\rho}}}$
Prop.	$\dot{\hat{\boldsymbol{x}}}(t) = \boldsymbol{f}\left(\hat{\boldsymbol{x}}(t), \hat{\bar{\boldsymbol{\rho}}}(t)\right) + \boldsymbol{u}(t)$ $\dot{\boldsymbol{P}}_{\boldsymbol{xx}}(t) = \mathbf{F}(t)\mathbf{P}_{\boldsymbol{xx}}(t) + \mathbf{P}_{\boldsymbol{xx}}(t)\mathbf{F}^T(t) + \mathbf{P}_{\boldsymbol{x}\bar{\boldsymbol{\rho}}}(t)\mathbf{B}^T_{\bar{\boldsymbol{\rho}}}(t) + \mathbf{B}_{\bar{\boldsymbol{\rho}}}(t)\mathbf{P}_{\bar{\boldsymbol{\rho}}\boldsymbol{x}}(t)$ $\dot{\boldsymbol{P}}_{\boldsymbol{x}\bar{\boldsymbol{\rho}}}(t) = \mathbf{F}(t)\mathbf{P}_{\boldsymbol{x}\bar{\boldsymbol{\rho}}}(t) + \mathbf{B}_{\bar{\boldsymbol{\rho}}}(t)\mathbf{P}_{\bar{\boldsymbol{\rho}}\bar{\boldsymbol{\rho}}}$

The equations of the CEKF are reported in Tab. 1. The equations in the first row describe the evolution of the state of the real system $\boldsymbol{x}$ and the readings of the sensors, $\boldsymbol{u}$ is the control force and $\boldsymbol{v}$ is the measurement noise with zero mean and covariance $\mathbf{R}$. The estimated state is integrated in time, along with its covariance, through the equations in the last row. The variation of the state covariance $\mathbf{P}_{xx}$ depends on $\mathbf{H}$, the Jacobian of $\boldsymbol{h}$. When a measurement is obtained by the sensor, the state and the covariance are updated accordingly, using the equations in the third row. $\mathbf{H}_x$ is the Jacobian of the measurement $\boldsymbol{h}$ and $\mathbf{K}$ is computed through the *gain* equation. The superscript + indicates the updated values of the variables, while the − the previous ones. The quantities peculiar to the Consider version of the EKF are:

- the *consider variable*: $\bar{\boldsymbol{\rho}}$;
- the cross-covariance between $\bar{\boldsymbol{\rho}}$ and the state of the system: $\mathbf{P}_{\bar{\boldsymbol{\rho}}\boldsymbol{x}}$ ($\mathbf{P}_{\boldsymbol{x}\bar{\boldsymbol{\rho}}} = \mathbf{P}^T_{\bar{\boldsymbol{\rho}}\boldsymbol{x}}$);
- the covariance matrix of $\bar{\boldsymbol{\rho}}$: $\mathbf{P}_{\bar{\boldsymbol{\rho}}\bar{\boldsymbol{\rho}}}$;
- the Jacobian of $\boldsymbol{f}$ with respect to $\bar{\boldsymbol{\rho}}$: $\mathbf{B}_{\bar{\boldsymbol{\rho}}}$.

4 Translational control

A control strategy based on Zero Effort errors [9] has been adopted. The Zero Effort Miss (ZEM) and the Zero Effort Velocity (ZEV) are defined as the error in position and velocity at the final instant if no control is applied:

$$\boldsymbol{ZEM}(t) = \boldsymbol{\rho}_d - \boldsymbol{\rho}_f(t); \quad \boldsymbol{ZEV}(t) = \dot{\boldsymbol{\rho}}_d - \dot{\boldsymbol{\rho}}_f(t) \tag{44}$$

where $\boldsymbol{\rho}_d$ and $\dot{\boldsymbol{\rho}}_d$ are the desired final position and velocity, while $\boldsymbol{\rho}_f(t)$ and $\dot{\boldsymbol{\rho}}_f(t)$ are the ones obtained if no control is applied from time t onwards. $\boldsymbol{\rho}_f(t)$ and $\dot{\boldsymbol{\rho}}_f(t)$ are obtained by integrating the motion from the current time t up to the final time t_f:

$$\boldsymbol{\rho}_f = \boldsymbol{\rho} + (t_f - t)\dot{\boldsymbol{\rho}} + \iint_t^{t_f} \ddot{\boldsymbol{\rho}}(\tau)\mathrm{d}\tau^2; \qquad \dot{\boldsymbol{\rho}}_f = \dot{\boldsymbol{\rho}} + \int_t^{t_f} \ddot{\boldsymbol{\rho}}(\tau)\mathrm{d}\tau \tag{45}$$

The control acceleration proportional to the ZEM/ZEV can be written as:

$$\boldsymbol{a}(t) = k_M(t)\,\boldsymbol{ZEM}(t) + k_V(t)\,\boldsymbol{ZEV}(t) \tag{46}$$

k_M and k_V can be tuned to minimize the fuel consumption while guaranteeing the impact. This optimization, if both the desired position and velocity are defined, gives:

$$\boldsymbol{a}(t) = 6/t_{go}^2\,\boldsymbol{ZEM}(t) - 2/t_{go}\,\boldsymbol{ZEV}(t) \tag{47}$$

If no constraint on the final velocity is given, the fuel-optimized acceleration is:

$$\boldsymbol{a}(t) = 3/t_{go}^2\,\boldsymbol{ZEM}(t) \tag{48}$$

The final instant has been defined as the moment at which the spacecraft is no more approaching the asteroid and is moving farther behind it. This occurs when the scalar product of the position and the velocity changes sign from negative to positive.

The gain increases with time and goes to infinity at the final instant. Therefore, a lower boundary on the estimated t_{go} is applied to prevent this risk. Also, it is affected by uncertainty, since it is computed from the estimated state. An estimation of its variance can be obtained using the linearized uncertainty propagation formula, that can give a safer estimation of the gains, substituting t_{go} with $t_{go} - 3\sigma_{t_{go}}$:

$$\sigma_{t_{go}}^2 \approx \frac{\partial t_{go}}{\partial \boldsymbol{x}} \Sigma_{\boldsymbol{x}} \left(\frac{\partial t_{go}}{\partial \boldsymbol{x}}\right)^T; \quad \frac{\partial t_{go}}{\partial \boldsymbol{x}} = \left[\frac{\partial t_{go}}{\partial \boldsymbol{\rho}} \;\; \frac{\partial t_{go}}{\partial \dot{\boldsymbol{\rho}}}\right] = \left[-\frac{\dot{\boldsymbol{\rho}}^T}{\dot{\boldsymbol{\rho}}\cdot\dot{\boldsymbol{\rho}}} \;\; -\frac{\boldsymbol{\rho}^T}{\dot{\boldsymbol{\rho}}\cdot\dot{\boldsymbol{\rho}}} + 2\frac{\boldsymbol{\rho}\cdot\dot{\boldsymbol{\rho}}}{(\dot{\boldsymbol{\rho}}\cdot\dot{\boldsymbol{\rho}})^2}\dot{\boldsymbol{\rho}}\right] \tag{49}$$

Perpendicular ZEM/ZEV In our mission the impact velocity is not imposed: in order to reach the asteroid, only lateral error are of interest. Accordingly, two new parameters that discard longitudinal errors are introduced ([8]):

- Perpendicular ZEM: error in position computed at the instant at which the spacecraft misses the asteroid, i.e. when the velocity is normal to the position.
- Perpendicular ZEV: part of the velocity that is normal to the position vector.

Fig. 3 Perpendicular ZEM/ZEV definition (A=asteroid, S=spacecraft)

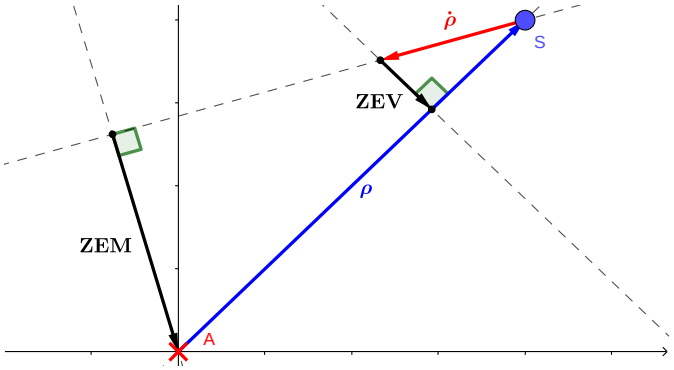

Neglecting the effects of the non-inertial frame, the motion with respect to the asteroid can be represented in a plane, as in Fig. 3, along with the newly introduced parameters, that can be computed as a function of the current state:

$$\boldsymbol{ZEM}_{\perp} = (\boldsymbol{\rho} \cdot \hat{\hat{\boldsymbol{\rho}}})\hat{\hat{\boldsymbol{\rho}}} - \boldsymbol{\rho}\,; \quad \boldsymbol{ZEV}_{\perp} = (\dot{\boldsymbol{\rho}} \cdot \hat{\boldsymbol{\rho}})\hat{\boldsymbol{\rho}} - \dot{\boldsymbol{\rho}} \tag{50}$$

The control formulation will then use the same gains as in the standard ZEM and ZEV definition (the optimality of this decision has not been proved).

5 Attitude control

Attitude control is needed to point the navigation camera towards the asteroid.

Control law The camera is considered to be mounted on the -z axis of the spacecraft: the goal of the controller is to have $\hat{\boldsymbol{z}} = \hat{\boldsymbol{\rho}}$. The implemented control law is:

$$\boldsymbol{m}^B = -k_q \ \mathrm{sgn}\left(q_w^e\right) \ \left[q_x^e \ q_y^e \ q_z^e\right]^T - k_\omega \, \boldsymbol{\omega}^B \tag{51}$$

where $\boldsymbol{m}^B$ is the control torque, k_q and k_ω are tunable gains and $(q_w^e, q_x^e, q_y^e, q_z^e)$ is the error quaternion. The angular velocity is introduced to stabilize the spacecraft. This law is based on the property that the imaginary part of a quaternion represents the rotation axis. The sign of q_w^e accounts for the situation in which $\hat{\boldsymbol{z}}$ and $\hat{\boldsymbol{\rho}}$ are more than 90 deg apart. The error between $\hat{\boldsymbol{\rho}}$ and $\hat{\boldsymbol{z}}$ can be computed using its definition:

$$\boldsymbol{q}^e = \cos(\theta/2) + \hat{\boldsymbol{e}} \sin(\theta/2) \tag{52}$$

where $\hat{\boldsymbol{e}}$ is the axis of rotation and θ is the rotation angle, that can be computed as:

$$\hat{\boldsymbol{e}} = (\hat{\boldsymbol{\rho}} \times \hat{\boldsymbol{z}}) \,/\, \|\hat{\boldsymbol{\rho}} \times \hat{\boldsymbol{z}}\|, \quad \cos\theta = \hat{\boldsymbol{\rho}} \cdot \hat{\boldsymbol{z}}, \quad \sin\theta = \|\hat{\boldsymbol{\rho}} \times \hat{\boldsymbol{z}}\| \tag{53}$$

Using trigonometric relations, the control law in Eq. 51 becomes:

$$\boldsymbol{m}^B = -\left(k_q / \sqrt{2\,(1 + \hat{\boldsymbol{\rho}} \cdot \hat{\boldsymbol{z}})}\right) \hat{\boldsymbol{\rho}}^B \times \hat{\boldsymbol{z}}^B - k_\omega \, \boldsymbol{\omega}^B \tag{54}$$

In the event that $\boldsymbol{\rho}$ and $\boldsymbol{z}$ are antiparallel, this gives an undefined result, and the error quaternion is built using an arbitrary unit vector normal to them as (q_x, q_y, q_z) and 0 as q_w. The gains have been chosen empirically as: $k_q = 0.05$ and $k_\omega = 2$.

6 Simulation and results

It is now possible to proceed with the software tool implemented to simulate the system and to validate the GNC strategy. Fig. 4 presents the software architecture, with the interconnections of the modules of the simulator. The dynamical model, the

image analyzer, the Kalman filters and the actuators are implemented in MATLAB® and Simulink® (lower part of the figure), while the image of the camera is rendered using Blender® (upper part). The programs communicate through a Python interface.

Fig. 4 Simulator architecture

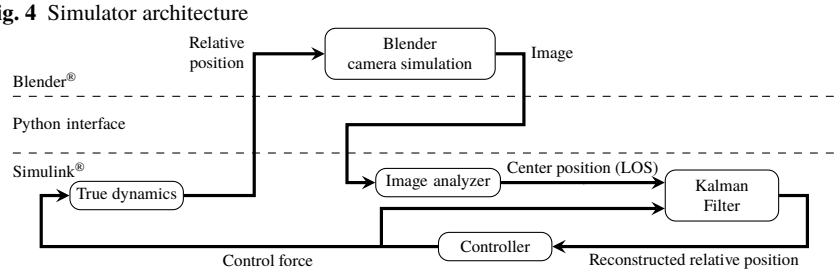

6.1 Simulation inputs

The position and velocity of the spacecraft and the orbital parameters of the asteroid at impact have been taken from Colombo et al. [3]. The initial data for the simulation have been obtained by backward propagation for 2000 s, starting from impact. The uncertainties applied to the initial conditions are reported in Tab. 2.

The parameters used for the simulation are:

- camera: FL 152.5 mm, sensor size 13.3 mm 1944 px, FOV 5°, 1 image every 20 s;
- asteroid 3D model: 101955 Bennu (from NASA 3D Resources);
- image analysis algorithm: parallel lines, with max. 20 fitting points;
- 3σ center of mass bias: $1/3$ of the expected asteroid diameter (550 m).

6.1.1 Modeling of sensors and actuators

An estimation of the variance of the measurement of the center of the asteroid has been obtained with a Monte Carlo analysis using the almost spherical asteroid Bennu. The distance between the estimated and the true centers has been related to the asteroid image size obtained by the analysis algorithm. This has shown that the estimation error is proportional to the size of the asteroid, with a ratio around 5%:

$$3\sigma[\text{PixelPos}_{\text{center}}] = 5\% \times \text{ImageSizePx} \tag{55}$$

which means that the 3σ error on the estimation of the asteroid center in the image is 5% of its size (in pixels). Using the optical relations that convert the pixels position in the image to angles, the variance of azimuth and elevation can be obtained as:

$$\sigma^2[\text{CameraAngle}] = (5\% \times \text{AstImgSize}/3 \times \text{PixelSize}/\text{FocalLength})^2 \tag{56}$$

The parameters for all the sensors are reported in Tab. 3. The errors are applied on each component of the quantity (i.e. coordinate, angle or quaternion component).

Table 2 Initial conditions

Quantity	Nominal value	Error (1σ)
Position	From impact orbit	$10/3$ km
Velocity	From impact orbit	$1/3$ m/s
Ang. velocity	Zero	1×10^{-4} rad/s
Quaternion	Cam. pointing to ast.	1×10^{-4}

Table 3 Sensor properties

Sensor	Error (1σ)	Rate
Camera angles	Variable (Eq. 56)	$1/20$ Hz
Star tracker	1×10^{-4} rad	$1/5$ Hz
Gyroscope	$0.1\,^{\circ}$/s	$1/5$ Hz

The spacecraft is considered to be equipped with thrusters and reaction wheels. A simplified actuator model has been implemented, where the required thrust and torque are subjected to limitations, as reported in Tab. 4.

Table 4 Actuator assumptions

Property	Value for thrust	Value for torque
Delay	5 s	0.1 s
Control frequency	0.2 Hz	10 Hz
Saturation limit	5 N	1 mN m
Control level quantization	0.5 N	0.01 mN m
Transient rate limit between control levels	0.5 N/s	1 mNm/s

6.2 Results

This section illustrates the results of Monte Carlo simulations performed to validate the model of the system and the developed GNC strategy. A set of 1000 initial conditions with Gaussian distribution has been generated and has been used for the simulations. For each set of initial conditions, the asteroid has been rotated in a different random attitude. No angular velocity has been applied to the asteroid.

Single run Before presenting the results of the Monte Carlo analysis, a single run has been executed to test the performances of the components of the simulator, including the proposed GNC strategy.

The real states to be estimated by the Kalman filters have been initially set to their nominal value increased by 1σ, in order to simulate the initial error.

Fig. 5 shows some example images acquired during the simulation. The labels report the time and distance to impact and the asteroid image diameter. The crosses represent: blue = CoB, yellow = fitted circle center, green = true center of the asteroid, red = target point as reconstructed by the filter. The search lines for the fitting points are in red and the obtained circle is white.

Fig. 5 Example images acquired during a simulation.

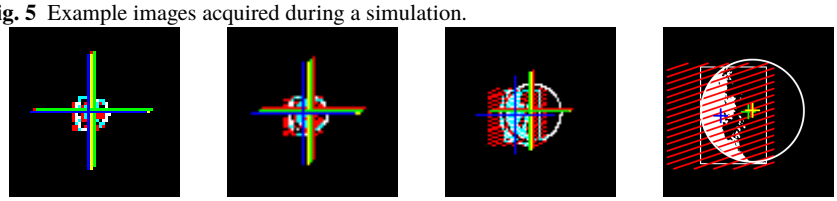

560 s, 1235 km, 10 px | 380 s, 838 km, 15 px | 200 s, 441 km, 28 px | 20 s, 44 km, 278 px

Fig. 6 Lateral position and velocity errors

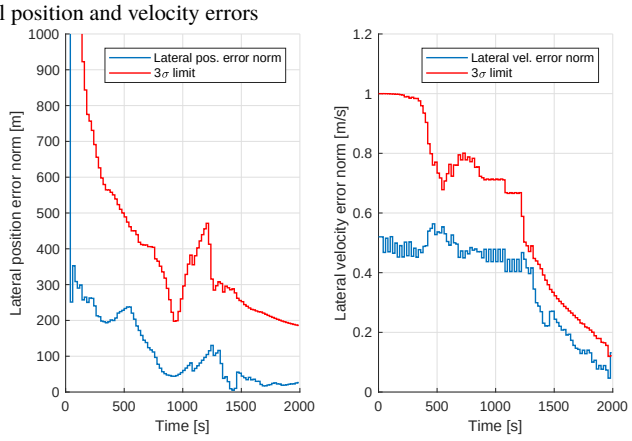

Fig. 7 Norm of angular velocity and quaternion errors

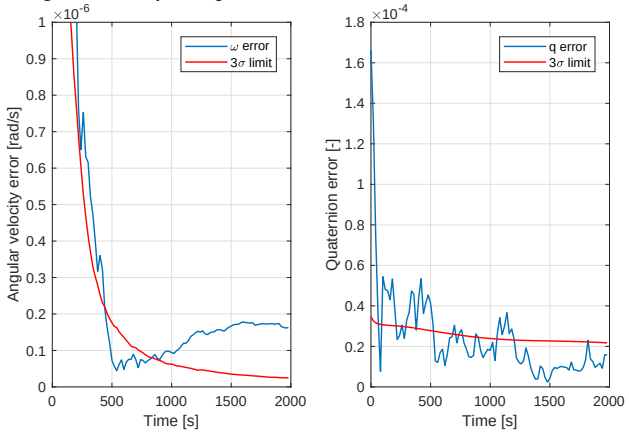

Fig. 6 reports the position error perpendicular to the LOS with its estimated 3σ limit. The initial significant error decreases during the approach to the asteroid, up to a value that is sufficiently low to grant impact. The error is always below the 3σ limit, therefore the filters have given consistent results.

The rotational error and its 3σ limit are plotted in Fig. 7. Considering how a rotation quaternion is defined, its error, that remains below 1×10^{-4}, can be associated to a rotation of about 0.01 deg, that is sufficiently low to point correctly towards the asteroid. Yet, it goes beyond the 3σ limit: this could be due to non-linearities in the attitude equations that should be analyzed in future work.

Fig. 8 Thrust

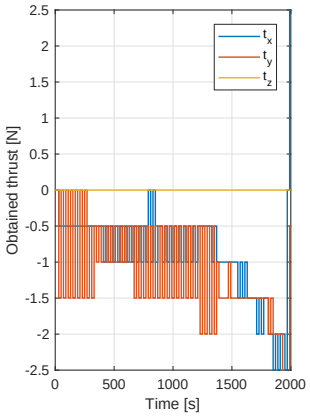

Fig. 9 Torque

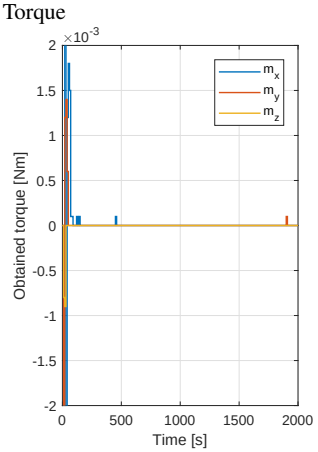

Fig. 8 reports the thrust profile until impact: no thrust is required along the z direction, which points towards the asteroid. This is the expected behavior of the adopted control strategy. After a transient, torque goes to zero (Fig. 9): this is expected since the spacecraft is moving along a trajectory almost aligned with the asteroid.

Monte Carlo analysis Running the Monte Carlo simulations, in 99.4% of the cases the asteroid is hit almost at his center, while in the 0.2% of them it is missed. This can be seen in Fig. 10, where the green curve represents the 3σ uncertainty ellipse of the points and the asteroid is schematically drawn as a circle, with center of mass at the axes origin. Fig. 12 and 13 report the distribution of impact points with respect to the distance from the center. Fig. 11 shows the time profiles of the impact error, in terms of norm of perpendicular ZEM. It decreases in time for all the simulations, meaning that the asteroid has been always detected and the control is working correctly.

Fig. 10 Impact points

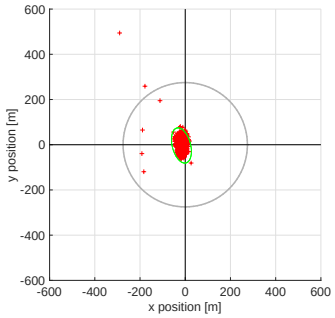

Fig. 11 $ZEM_{\perp}$

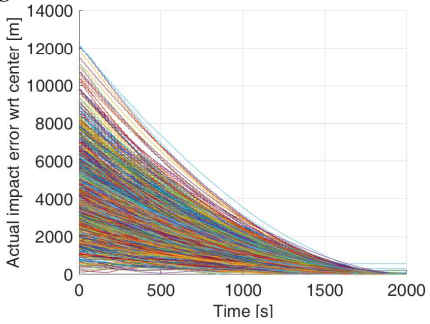

Fig. 12 Density of impact points

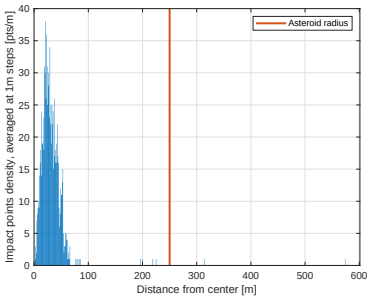

Fig. 13 Cumulative distribution of impact p.

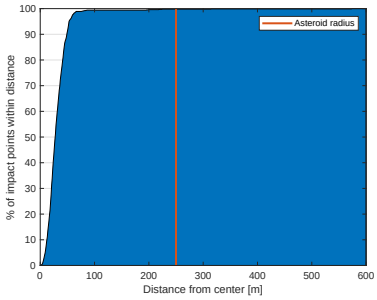

7 Conclusions and future work

The aim of this work was to design a GNC strategy for a reference impactor mission for asteroid deflection and to evaluate its performances by developing a computer simulator. Within the considered initial error in position and velocity, the implemented GNC strategy shows good performances and allows to impact the asteroid in almost all the simulated cases. Still, the simulated test case is very specific and it is then necessary to test the GNC strategy on different mission scenarios.

The developed software is versatile: the flexibility of the Simulink® model and the possibility to tune the parameters of the system allow the user to test different mission scenarios with minor modifications.

Significant amount of work shall be dedicated to develop a more realistic simulator and to perform a complete mission analysis.

The Blender® model used to simulate the navigation camera shall be improved, implementing the stars in the background and other phenomena that affect the image acquired (e.g. asteroid magnitude, camera aperture, noise). Then, the effectiveness of the image analysis algorithm must be tested using the improved rendering model.

A more precise estimation of the typical initial uncertainties attainable in this kind of missions will be performed. Alternatively, the initial error could be gradually enlarged to find the maximum affordable value.

The simulations have been performed considering that the GNC is active only for the last 2000 s. Yet, some cameras are able to detect the asteroid earlier: the possibility of improving the results by executing GNC operations starting at a different time-to-impact will be evaluated.

A natural continuation of this work will also be the assessment of the deflection effect attained after impact, considering the achieved impact position and velocity.

In addition, future work will be devoted to run the GNC strategy in a processor-in-the-loop framework to verify its on-board applicability.

Acknowledgements The authors would like to acknowledge the support provided by C. Colombo, E. Vellutini, M. Castronuovo, M. Albano, R. Bertacin, A. Gabrielli, E. Perozzi and G. Valsecchi for the definition of the test case scenario.

References

1. P. Berner, R. Toms, K. Trott, F. Mamaghani, D. Shen, C. Rollins, and E. Powell. Technical Concepts Orientation, Rotation, Velocity and Acceleration, and the SRM. 2008.
2. I. Carnelli, A. Gàlvez, and D. Izzo. Don Quijote: a NEO deflection precursor mission. *NASA Workshop: Near–Earth Object Detection, Characterization and Threat Mitigation*, 2006.
3. C. Colombo, M. Albano, R. Bertacin, M. M. Castronuovo, A. Gabrielli, E. Perozzi, G. Valsecchi, and E. Vellutini. Mission analysis for two potential asteroids threat scenarios: optimal impact strategies and technology evaluation. In *68th IAC*, pages 1–12. IAF, 2017.
4. J. L. Crassidis and J. L. Junkins. *Optimal estimation of dynamic systems*. CRC Press, 2012.
5. P. Di Lizia, M. Massari, F. Cavenago, A. Wittig, and L. Summerer. Assessment of onboard DA state estimation for spacecraft relative navigation Final Report. Technical report, ESA, 2017.
6. L. Drube. SMPAG Roadmap of Relevant Research for Planetary Defense. 2018.
7. A. Gàlvez, I. Carnelli, P. Michel, A. F. Cheng, C. Reed, S. Ulamec, J. Biele, P. A. Abell, and R. Landis. AIDA: The Asteroid Impact & Deflection Assessment Mission. *European Planetary Science Congress*, 2013.
8. Y. Guo, M. Hawkins, and B. Wie. Applications of Generalized ZEM/ZEV Feedback Guidance Algorithm. *Journal of Guidance, Control, and Dynamics*, 36(3):810–820, may 2013.
9. M. Hawkins, Y. Guo, and B. Wie. ZEM/ZEV Feedback Guidance Application to Fuel-Efficient Orbital Maneuvers Around an Irregular-Shaped Asteroid. In *AIAA GNC Conference*, 2012.
10. D. G. Kubitschek, N. Mastrodemos, R. A. Werner, B. M. Kennedy, S. P. Synnott, G. W. Null, S. Bhaskaran, J. E. Riedel, and A. T. Vaughan. Deep Impact autonomous navigation: The trials of targeting the unknown. In *AAS*, volume 125, pages 381–406. JPL, NASA, feb 2006.
11. T. Kubota, T. Hashimoto, J. Kawaguchi, M. Uo, and K. Shirakawa. Guidance and Navigation of Hayabusa Spacecraft for Asteroid Exploration and Sample Return Mission. In *2006 SICE-ICASE International Joint Conference*, pages 2793–2796. IEEE, 2006.
12. H. Schaub and J. L. Junkins. *Analytical mechanics of space systems*. 2003.
13. D. Woodbury and J. L. Junkins. On the Consider Kalman Filter. In *AIAA GNC Conf.*, 2010.